MedChemComm

CONCISE ARTICLE

View Article Online
View Journal | View Issue

Cite this: *Med. Chem. Commun.*, 2015, **6**, 1003

Structure-based virtual screening for fragment-like ligands of the G protein-coupled histamine H_4 receptor†

Enade P. Istyastono,‡[ab] Albert J. Kooistra,‡[a] Henry F. Vischer,[a] Martien Kuijer,[a] Luc Roumen,[a] Saskia Nijmeijer,[a] Rogier A. Smits,[c] Iwan J. P. de Esch,[a] Rob Leurs[a] and Chris de Graaf*[a]

Received 16th January 2015,
Accepted 26th March 2015

DOI: 10.1039/c5md00022j

www.rsc.org/medchemcomm

We have explored the possibilities and challenges of structure-based virtual screening (SBVS) against the human histamine H_4 receptor (H_4R), a key player in inflammatory responses. Several SBVS strategies, employing different H_4R ligand conformations, were validated and optimized with respect to their ability to discriminate small fragment-like H_4R ligands from true inactive fragments, and compared to ligand-based virtual screening (LBVS) approaches. SBVS studies with a molecular interaction fingerprint (IFP) scoring method enabled the identification of H_4R ligands that were not identified in LBVS runs, demonstrating the scaffold hopping potential of combining molecular docking and IFP scoring. Retrospective VS evaluations against H_4R homology models based on the histamine H_1 receptor (H_1R) crystal structure did not give higher enrichments of H_4R ligands than H_4R models based on the beta-2 adrenergic receptor (β_2R). Complementary prospective SBVS studies against β_2R-based and H_1R-based H_4R homology models led to the discovery of different new fragment-like H_4R ligand chemotypes. Of the 37 tested compounds, 9 fragments (representing 5 different scaffolds) had affinities between 0.14 and 6.3 μM at the H_4R.

Introduction

The histamine H_4 receptor (H_4R), belonging to the family of G protein-coupled receptors (GPCRs),[1] has been reported to play an important role in allergic and inflammatory processes.[2–6] So far, one H_4R ligand has entered Phase II clinical trials,[2,4] but no marketed drug currently targets this receptor. The quest to find new ligands for H_4R therefore remains attractive. Most H_4R ligands (including compounds JNJ777120 (**2**) and VUF10497 (**3**); Fig. 1) have resulted from high-throughput screening (HTS) campaigns and subsequent medicinal chemistry programs.[4–8]

Fragment-based drug discovery (FBDD)[9–11] is a new paradigm in drug discovery that utilizes small molecules (molecular weight ≤300 Dalton, heavy atoms ≤22)[12–14] as starting points for hit optimization. Within the context of FBDD, fragment-based screening is a more efficient way to sample chemical space and generally yields higher hit rates than

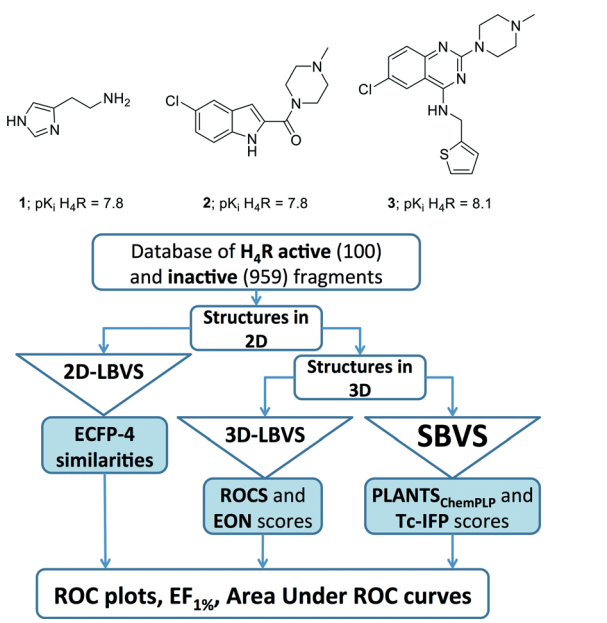

Fig. 1 Structure and the biological activity of histamine (**1**), JNJ7777120 (**2**), and VUF10497 (**3**).[7,8,81] and the flowchart of approaches employed in the retrospective VS protocols. See **Experimental section** for more details.

[a] *Division of Medicinal Chemistry, Amsterdam Institute for Molecules, Medicines and Systems (AIMMS), Faculty of Exact Sciences, VU University Amsterdam, De Boelelaan 1083, 1081 HV Amsterdam, The Netherlands. E-mail: C.de.Graaf@vu.nl*
[b] *Center for Environmental Studies Sanata Dharma University (CESSDU), Division of Drug Design and Discovery, Faculty of Pharmacy, Universitas Sanata Dharma, Depok, Sleman, Yogyakarta 55282, Indonesia*
[c] *Griffin Discoveries B.V., De Boelelaan 1083, 1081 HV Amsterdam, The Netherlands*

† Electronic supplementary information (ESI) available. See DOI: 10.1039/c5md00022j

‡ These authors contributed equally.

classical high-throughput screening (HTS) campaigns of larger, drug-like compound.[11,14,15] Biochemical and biophysical fragment screening studies of small chemical libraries (*circa* 25–1010 compounds) against different GPCRs have been reported with 0.4–14% hit rates yielding several new chemical starting points for fragment-based GPCR ligand optimization.[14,16–22] So far only few experimental screens of the same fragment library against multiple GPCR targets have been reported[14,16] that can provide information about the molecular determinants of GPCR-ligand selectivity by fragment-based chemogenomics analyses.[14,23]

Virtual fragment screening approaches, the *in silico* prediction of fragment binding to protein binding sites that has the potential to explore protein–ligand space more extensively, have been successfully applied to identify new fragment-like ligands for several GPCR targets, with 20–73% hit rates (% of experimentally tested *in silico* hits with detectable binding affinity).[18,20,22,24–27] While ligand-based virtual screening methods often only allow the identification of chemically similar ligands, protein-based virtual screening approaches potentially offer the possibility of scaffold hopping, the discovery of ligands with new chemical functional groups.[24,28–30] GPCR structure-based virtual fragment screening (SBVFS),[18,22,24–26] the identification of smaller fragment-like molecules by docking simulations[31] of large chemical databases in GPCR 3D structures, is however, still challenging and several problems have been identified including: (i) *Conformational sampling problem*: proper consideration of protein flexibility in docking simulations is difficult and small differences between experimentally-determined crystal structures, as well as structural inaccuracies in protein homology models, can affect sampling and scoring of different GPCR-ligand conformations.[32–35] In particular, docking small fragments in a large binding pocket may result in multiple distinct binding modes with similar docking scores.[36–38] (ii) *Scoring problem*: the ability of docking scoring functions to rank ligand docking poses in order to predict ligand binding modes and discriminate ligands from inactive molecules depends on the properties of the GPCR binding site and fine details of GPCR-ligand interactions.[27,30,34,39,40] Moreover, docking scoring functions are generally not optimized for discriminating docking poses of small fragment-like molecules with comparable energy scores.[36–38]

(iii) *Training problem*: There are limited experimental data on true inactive fragment-like compounds that are required to optimize and validate structure-based virtual screening approaches.[14,20,25] Furthermore, experimentally-determined crystal structures of the targeted protein in complex with fragment-like ligands are often lacking, and therefore cannot be used to validate structure-based virtual fragment screening approaches.

Several recent developments in the field of GPCR structural biology and FBDD can help to address these conformational sampling, scoring, and training problems associated with structure-based virtual fragment screening. In the past eight years crystal structures of 27 different GPCRs have been solved,[41–43] including the adrenergic beta-2-receptor (β_2R)[44] and histamine H_1 receptor (H_1R).[45] Structure-based virtual screening (SBVS) campaigns against GPCR crystal structures (in particular β_2R,[46] adenosine A_{2A} receptor (A_{2A}R),[47,48] dopamine D_3 receptor (D_3R),[39] 5-hydroxytryptamine receptor 2B ($5HT_{2B}$R),[49] and H_1R[24] have resulted in relatively high hit rates (24–73%) and yielded several small fragment-like ligands (≤22 heavy atoms).[18,22,27] Although some successful SBVS studies with high hit rates (>20%) have also been reported based on GPCR homology models,[39,50,51] the GPCR crystal structures seem to offer improved opportunities to push the limits of structure-based ligand discovery and design,[18,20,22,24,27,30,52] including the application of virtual fragment screening to GPCRs.[22,27,30,52] The increasing number of GPCR crystal structures for different GPCR subfamilies furthermore offer higher-resolution templates for modeling the structures of GPCRs for which crystal structures have not yet been solved.[30,32,33,35,53] Three-dimensional H_4R-ligand binding-mode models have been derived by (combining) ligand-based and protein-based modeling approaches, ligand structure–activity relationships, and site-directed mutagenesis studies.[54–61] Experimentally validated homology models of human H_4R have been constructed based on bovine Rhodopsin (bRho),[54–56] β_2R,[58,59,62] and more recently the H_1R crystal structure.[26,60,61] Although H_4R shares more ligands with H_1R than with β_2R,[23] sequence identity between the H_4R and H_1R binding site (28%) is only slightly higher than between the H_4R and β_2R binding site (26%, ESI† Fig. S1).[23] Interestingly, H_4R models based on β_2R and H_1R crystal structure templates were equally successful in explaining H_4R mutation data, while H_1R-based H_4R models could better explain ligand SAR than β_2R-based H_4R homology models.[60]

The challenges in structure-based virtual screening against GPCR homology models have been demonstrated by previous H_4R virtual screening campaigns.[26,56] In a large scale virtual screening study of more than 5 million compounds against a bRho-based H_4R model (refined with histamine), 255 *in silico* hits were selected for experimentally testing, of which 11 had low affinity (>10 μM) and 5 had K_i values of 10 μM or lower (compounds 4–7, ESI† Fig. S2).[56] Although the discovery of fragment-like molecules was not the aim of this study, most of the identified ligands were fragment-like.[12–14] In another study retrospective virtual screening studies against MD simulation snapshots of a H_1R-based H_4R model (refined with JNJ-777120), allowed for the identification of representative H_4R structures that gave optimal enrichments of known H_4R ligands *versus* decoy molecules compared to the initial H_4R homology model.[34] This ensemble docking approach was subsequently applied in a prospective virtual screening campaign in which 50 *in silico* hits were selected for experimental testing. Nine of the fragment hits had low H_4R affinity (>10 μM) and one fragment (compound **8**, ESI† Fig. S2) had a K_i value of 8 μM.[26]

The aim of this study is to investigate the possibilities and limitations of structure-based virtual screening for the identification of new fragment-like ligands for H_4R. *Conformational*

sampling problems will be addressed by the construction of different three-dimensional receptor models of the human H_4R with different ligands (compounds **1–3**, Fig. 1),[7,8,59,63] based on two different crystal structure templates (β_2R[44] and H_1R[45]), and by the consideration of different molecular dynamics simulation snapshots. Although crystal structures of several aminergic GPCRs are available to construct H_4R homology models (*i.e.* β_1R, β_2R, D_3R, H_1R, M_2R, M_3R, $5HT_{1B}R$, $5HT_{2B}R$),[44,45,64–68] β_2R and H_1R are selected as H_4R modelling templates because: i) this allows us to further build from our β_2R-based and H_1R-based H_4R modelling studies;[60] ii) H_1R is the crystallized GPCR that shares the highest number of ligands with H_4R,[23] and iii) β_2R has been a frequently used crystal structure target[46,69–71] and GPCR modelling template[26,39,72] in prospective structure-based virtual screening studies in the past few years.[27] *Scoring* and *training problems* will be addressed by: i) the use of a molecular interaction fingerprint (IFP) scoring method that considers protein–ligand interaction similarity to experimentally validated H_4R-ligand binding-mode models consistent with H_4R ligand structure–activity and structure–selectivity relationship and site-directed mutagenesis (SDM) studies. ii) the retrospective validation, comparison, and optimization of different virtual screening approaches based on a training set containing not only known H_4R fragment-like ligands but also experimentally validated *inactive* fragments.[13,17] The IFP scoring method has been shown to outperform energy-based scoring methods in previous GPCR structure-based virtual (fragment) screening studies[36,73,74] and enable the identification of new chemical ligand scaffolds.[18,24,25] Optimal structure-based virtual screening approaches identified in the current study will therefore be compared with two-dimensional (2D) and three dimensional (3D) ligand-based virtual screening methods. Although pharmacophore-based virtual screening techniques were not considered in the current study, it should be noted that scaffold hopping potential of pharmacophoric methods is also well recognized,[75] as for example demonstrated in virtual screening studies for new histamine H_3 receptor ligands.[25] Systematic analysis and comparison of hit sets in both retrospective and prospective virtual screening studies will provide insights into the relative performance and complementarity of different virtual screening approaches in the identification of novel fragment-like H_4R ligands. Fragment training sets of experimentally determined binders/actives and non-binders/inactives have been previously used for the optimization and validation of ligand-based and protein-based FLAP pharmacophore models for the discovery of new fragment-like H_3R ligands[25] and the evaluation of different consensus-scoring strategies for ligand-based virtual screening for fragment-like H_1R and H_4R ligands.[76] In the current study, training sets of experimentally determined binders and non-binders have been used for the first time to optimize and validate protein structure-based virtual screening methods. The lessons learned from our comparative retrospective and prospective virtual fragment screening studies can be used as a blueprint for future structure-based virtual (fragment) screening studies.

Results

Retrospective evaluation ligand-based and structure-based virtual screening methods

A dedicated training set, containing 100 unique fragment-like H_4R ligands from our in-house fragment library[14,17] and the ChEMBL database[77] and 959 fragments inactive at human H_4R,[14,17] was used for retrospective validation of different structure-based and ligand-based (LBVS) virtual screening approaches (Fig. 1). The chemical structures and binding modes of the H_4R ligands histamine (**1**), JNJ7777120 (**2**), and VUF10497 (**3**) (Fig. 1) were used as reference compounds in the retrospective VS runs. These selected ligands represent different steps in H_4R ligand-optimization strategies in the past years:[4–6] (i) modification of the basic amine, and (ii) substitution of the imidazole ring with bioisosteres.[4] Histamine (**1**) is the endogenous ligand of H_4R and JNJ7777120 (**2**) is the first published selective non-imidazole H_4R ligand, a biased agonist for the β-arrestin pathway,[78,79] and both have served as reference compounds in previous ligand-based and protein-based H_4R virtual screening and ligand design studies.[8,26,56,80] VUF10497 is a high affinity H_4R inverse agonist and is representative for a series based on an in-house discovered H_4R scaffold.[8,63]

The binding modes of the reference compounds in the H_4R binding pocket were derived following the information extracted from previous structure–activity relationship and mutation studies on H_4R.[4,59,61,82] All compounds display H-bond interactions to $D94^{3.32}$ and $E182^{5.46}$.[4,59] Mutagenesis studies have indicated that these residues are essential H-bond acceptor interaction points for H_4R ligands[54,55,60] and suggest that $D94^{3.32}$ and $E182^{5.46}$ form H-bond interaction networks with $Q347^{7.42}$ and $N147^{4.57}$, respectively.[58,59] The transmembrane (TM) binding pocket is very similar in both H_4R models based on β_2R and H_1R (Fig. 2),[4,59,82] but there are differences in the second extracellular loop (EL2).[74,83,84] These differences slightly affect the binding orientation of JNJ7777120 (**2**) (Fig. 2),[58] while the binding poses of histamine (**1**)[58,85] and VUF10497 (**3**) remain very similar (Fig. 2). In the β_2R-based H_4R model the chlorine atom of JNJ7777120 (**2**) is located between EL2 (F168), TM5 ($L175^{5.39}$), and TM6 ($T323^{6.55}$), while in the H_1R-based model the chlorine atom of JNJ7777120 is accommodated between TM5 ($L175^{5.39}$ and $T178^{5.42}$) and EL2 (F168) (Fig. 2).[4,58] It should be noted that the functional effect of these ligands vary considerably, from inverse agonist (VUF10497 (**3**)) to biased agonist (JNJ-7777120 (**2**)) to full agonist (histamine). Clearly, the fragments to be identified in these VS efforts do not represent optimized compounds. It is apparent from literature that even the smallest structural changes of a ligand during hit or lead optimization (*i.e.*, for fragments but also for drug-like molecules) can completely alter the functional activity from agonist to antagonist and *vice versa*.[86,87] Furthermore, the functional activity is

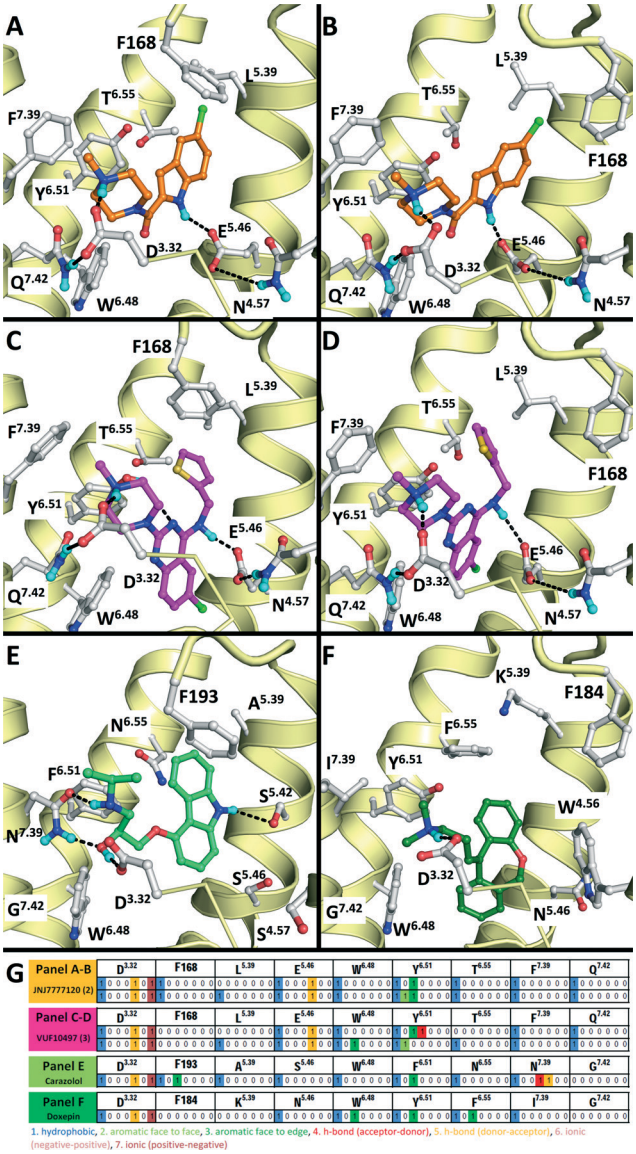

Fig. 2 Comparison of β_2R–carazolol (light green) crystal structure[44] (**E**) based H_4R models (**A**, **C**) and H_1R–doxepin dark green) crystal structure (**F**) based H_4R models[45] (**B**, **D**). H_4R models are constructed with JNJ7777120 (**2**, orange carbon atoms, **A** and **B**) and VUF10497 (**3**, magenta, **C** and **D**). Protein–ligand interaction fingerprints (IFPs) of the binding modes in **A**–**F** are presented in **G**. The backbone of TM helices 4, 5, 6, and 7 are represented by yellow tubes and part of TM3 is shown as ribbon (the top of the helix is not shown for clarity). Important binding residues identified previously[4,55,56,59,61,82] are depicted in grey.

highly dependent on the species investigated and on the signalling pathways studied.[58,78,79,88–90] On a protein molecular level this probably means that the differences between agonists and antagonists can be relatively small, but the effect these changes can have on the conformation (activation state) of the receptor can be big.[27] For this fragment-based VS campaign, we have chosen not to focus on the functional effect of the ligands, but on the affinity for H_4R.

The retrospective VS flowchart is presented in Fig. 1. 2D-LBVS and 3D-LBVS similarity searches of the test set of H_4R binders and non-binders were ranked according to ECFP-4 (Tanimoto score)[91] and ROCS-EON (Comboscore)[92] similarity against reference ligands (**1**–**3**).[24] In the SBVS runs, compounds were docked against molecular dynamics simulation snapshots of β_2R-based[44,58,59] and H_1R-based[45] H_4R homology models. The resulting docking poses were ranked subsequently using $PLANTS_{ChemPLP}$ [93] and interaction fingerprint (IFP)[36,74,94] similarity scores to reference binding modes of ligands **1**–**3** (Fig. 2). ROC plots (% true positives (TP) *versus* % false positives (FP) in the ranked database)[74] of the retrospective analysis of 2D-LBVS, 3D-LBVS and SBVS hit lists are presented in Fig. 3. The enrichment factor 1% ($EF_{1\%}$) of the VS protocols together with the area under ROC curves are summarized in Table 1.[95–97]

Table 1 and Fig. 3 indicate that 2D-LBVS, 3D-LBVS and SBVS-IFP can give a good early enrichment. SBVS using $PLANTS_{ChemPLP}$ scoring on the other hand resulted in

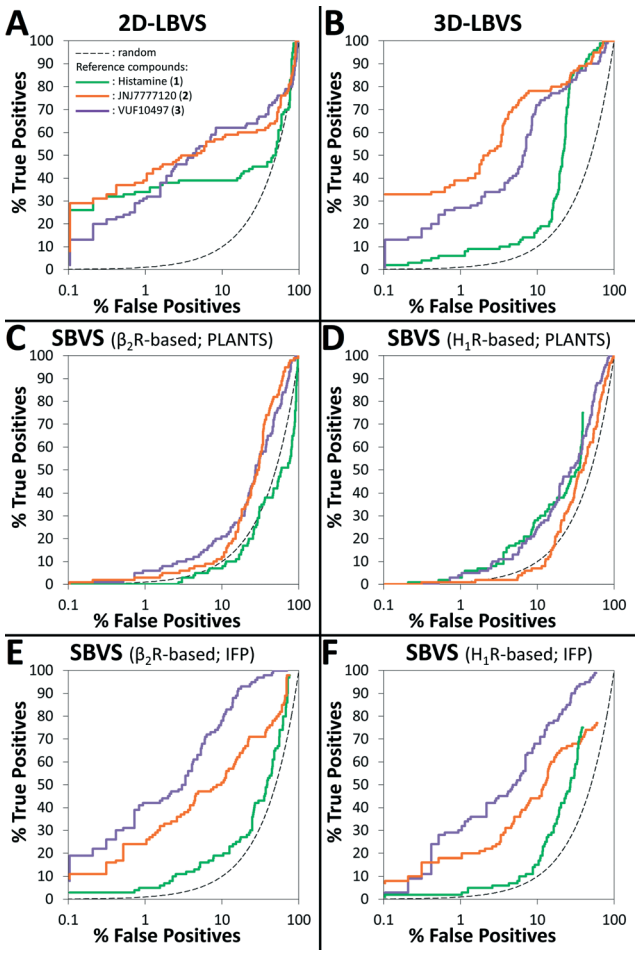

Fig. 3 Graphs of % true positives (fragment-like H_4R ligands) *vs.* % false positives (fragments that do not bind H_4R) in the ranked database resulted from 2D-LBVS (**A**), 3D-LBVS (**B**), β_2R-based SBVS ranked by $PLANTS_{ChemPLP}$ score (**C**), H_1R-based SBVS ranked by $PLANTS_{ChemPLP}$ score (**D**), β_2R-based SBVS re-ranked by Tc-IFP score (**E**), and H_1R-based SBVS re-ranked by Tc-IFP score (**F**) based on histamine (**1**, green), JNJ-7777120 (**2**, orange), and VUF10497 (**3**, purple) reference ligands (**A**–**B**) and ligand-H_4R IFPs (**C**–**F**).

Table 1 The enrichment factor 1% ($EF_{1\%}$) and the area under ROC curves (AUC) of the VS protocols

VS protocol	References: Histamine (1) $EF_{1\%}$	Histamine (1) AUC (CI[a])	JNJ7777120 (2) $EF_{1\%}$	JNJ7777120 (2) AUC (CI[a])	VUF10497 (3) $EF_{1\%}$	VUF10497 (3) AUC (CI[a])
Ligand-based VS						
2D[b]	32.6	0.61 (0.54–0.98)	37.4	0.71 (0.64–0.78)	29.7	0.73 (0.66–0.80)
3D[c]	5.7	0.77 (0.74–0.81)	37.4	0.89 (0.85–0.93)	25.9	0.85 (0.81–0.90)
β_2R-based SBVS						
PLANTS[d]	0.0	0.58 (0.52–0.65)	2.9	0.69 (0.64–0.73)	5.7	0.66 (0.61–0.71)
Tc-IFP[e]	4.8	0.62 (0.57–0.67)	23.0	0.78 (0.73–0.84)	40.3	0.94 (0.92–0.97)
H_1R-based SBVS						
PLANTS[f]	2.9	0.67 (0.62–0.72)	1.0	0.58 (0.52–0.63)	3.8	0.68 (0.63–0.73)
Tc-IFP[g]	1.9	0.68 (0.63–0.73)	17.3	0.73 (0.66–0.79)	28.8	0.89 (0.86–0.93)

[a] Confidence interval of the AUC with level of confidence of 95% calculated using pROC packages in R statistical computing software.[95] [b] Fig 3A. [c] Fig 3B. [d] Fig 3C. [e] Fig 3D. [f] Fig 3E. [g] Fig 3F.

significantly lower enrichments. The 2D-LBVS runs result in a lower global virtual screening accuracy (reflected by the area under ROC curves) compared to the 3D approaches. On the other hand, low early enrichments as well as global virtual screening accuracies were obtained with the 3D approaches using histamine (1) as the reference compound. JNJ7777120 (2) appeared to be the best reference for 2D- and 3D-LBVS runs, while the VUF10497 (3) binding mode performed as the best reference for post-processing SBVS docking simulations. Interestingly, β_2R-based SBVS resulted slightly higher enrichments compared to H_1R-based SBVS.

We furthermore evaluated the ability of the different methods to identify "novel" fragment-like molecules (Fig. 4). In our retrospective virtual screening studies "novel" fragments were defined as compounds that have an ECFP-4 Tanimoto similarity (Tc-ECFP4) score to any reference compounds of less than 0.26.[98] β_2R-based SBVS yielded the most novel hits (Fig. 4C), followed by H_1R-based SBVS (Fig. 4D) and 3D-LBVS (Fig. 4B).

Histamine (1) (and histamine-H_4R binding modes) was only a suitable reference in 2D-LBVS runs (Fig. 4E), while both JNJ7777120 (2) and VUF10497 (3) were good references in different virtual screening protocols (Fig. 4F–G). Fig. 4E–H show clear overlaps between 2D- and 3D-LBVS by using JNJ7777120 (2) or VUF10497 (3) as the reference. Fig. 4F shows a high number of hits only identified by the LBVS studies, which were not identified in the SBVS studies by using JNJ7777120 (2) as the reference. Fig. 4F shows that the use of JNJ7777120 (2) in the SBVS studies increases the chance to retrieve "novel" H_4R fragments. The highest number of shared hits between all SBVS methods were retrieved in the VUF10497-based SBVS studies (Fig. 4G). Collection of the hits that were retrieved at a 1% false positive rate using all references results in the Venn diagram presented in Fig. 4H. Although most active H_4R fragments were retrieved using LBVS, SBVS provided a higher probability of retrieving "novel" H_4R fragments.

Based on the results of our retrospective virtual screening studies, we performed the prospective SBVS campaigns using the β_2R-based[44,58,59] and H_1R-based[45] H_4R homology models in complex with reference ligands 2 and 3 (Fig. 3 and 5).

Prospective structure-based virtual screening studies to discover new H_4R ligands

The SBVS approach against the β_2R-based H_4R model was determined to be the best method in identifying novel fragment-like ligands (Fig. 4). We therefore used this model in a prospective *in silico* screening study to discover new

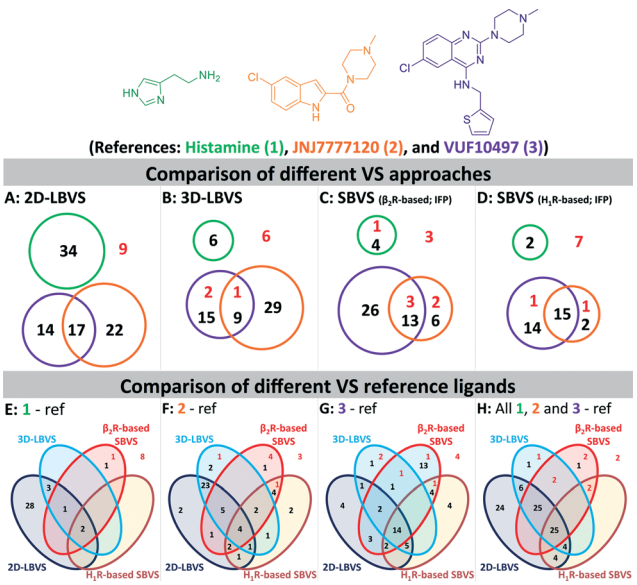

Fig. 4 Venn diagrams of the number of actives at a 1% false positive rate resulted in 2D-LBVS (**A**), 3D-LBVS (**B**), β_2R-based SBVS re-ranked by Tc-IFP score (**C**), and H_1R-based SBVS re-ranked by Tc-IFP score (**D**). The circles proportionally indicate the number of actives at a 1% false positive rate based on histamine (**1**, green), JNJ777120 (**2**, blue), or VUF10497 (**3**, purple) references (Panels **A**–**D**). Venn diagrams of the number of actives at a 1% false positive rate resulted in all used VS methods using histamine (**1**, panel **E**), JNJ777120 (**2**, panel **F**), VUF10497 (**3**, panel **G**) or consensus references (panel **H**). Red numbers indicate active H_4R fragments in the database that have an ECFP-4 Tanimoto similarity score of less than 0.26 to any of the references.[98]

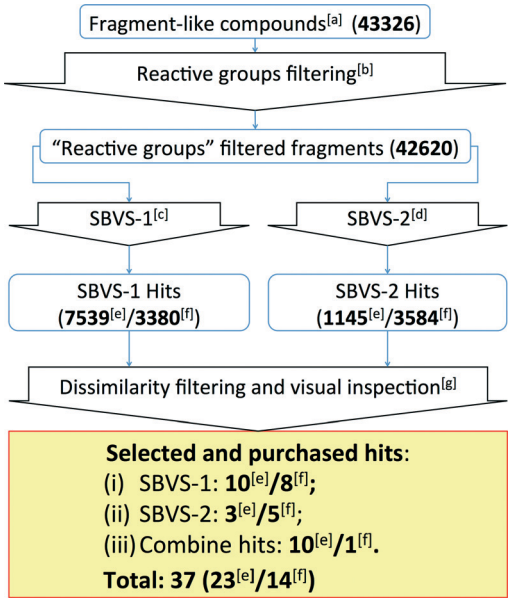

Fig. 5 Flowchart of the β_2R-based and H_1R-based prospective SBVS campaigns. See **Experimental section** for more details. [a]Fragment-like compounds collected from the ZINC database.[37,99] [b]Filtering fragments containing plausible reactive/toxic groups.[100] [c]SBVS with JNJ7777120 (**2**) as the reference compound.[7,56,80] [d]SBVS with VUF10497 (**3**) as the reference compound.[8,56,63] [e]Results from the β_2R-based prospective SBVS studies. [f]Results from the H_1R-based prospective SBVS studies. [g]Fragments with ECFP-4 Tanimoto similarity score of less than 0.40 to any of the H_4R ligands used in the retrospective VS.[24] In the H_1R-based prospective SBVS campaigns, H_4R purchased hits from the β_2R-based prospective SBVS studies were added as the reference compounds in the dissimilarity filtering.

active H_4R fragments from a subset of fragment-like (and commercially-available) molecules extracted from the ZINC database (Fig. 5, ESI† Table S1).[99] Based on the results of the retrospective VS studies (Table 1, Fig. 4), two β_2R-based H_4R models and their corresponding IFP references were used in parallel: i) The first SBVS run was rescored using the Tanimoto coefficient-based IFP similarity (Tc-IFP) against the JNJ7777120 (**2**) customized H_4R model (SBVS-1), and ii) A second *in silico* screen rescored using Tc-IFP against the VUF10497 (**3**) based H_4R model (SBVS-2) (Fig. 4). In the retrospective VS studies, the re-scoring using Tc-IFP clearly shows the increase of SBVS quality compared to the ones using $PLANTS_{ChemPLP}$ scores (Table 1, Fig 3). Our retrospective validation studies showed that many of the "novel" ligands (*i.e.*, not identified with 2D ligand-based VS) were identified in the SBVS-1/SBVS-2 consensus hit list and the SBVS-1 hit list (Fig. 4E).

We therefore especially selected compounds from these lists in our prospective VS campaign: 23 fragments were selected (ESI† Fig. S3 and ESI† Table S2) and purchased, from which 6 were experimentally confirmed as H_4R ligands (Table 2), including three piperazine-benzofuropyrimidines with submicromolar affinity (**9a–c**), and three pyrimido-indole containing fragments with micromolar affinity (**10a–c**). None of the validated hits had detectable binding affinity for β_2R, demonstrating that the SBVS was not biased towards the structural template[39] used to construct the H_4R homology models (Table 2). Following the successful efforts in the discovery of novel H_4R fragments by using the β_2R-based H_4R model, we subsequently performed similar SBVS campaigns employing H_1R-based H_4R model (Fig. 5). In order to increase our chances of finding ligands with a different chemotype we added the newly discovered H_4R hit ligands as references compounds in the dissimilarity filter (Fig. 5). Fourteen fragments were selected and purchased (ESI† Fig. S4 and ESI† Table S3). Three of the hits from the H_1R-based prospective SBVS (**11–13**) were experimentally confirmed as H_4R ligands (Table 3). In total, 37 fragments were selected and purchased. Nine out of these 37 purchased fragments were confirmed as H_4R ligands with binding affinities between 0.14 and 6.9 μM (Tables 2–3; Fig. 6). The hits represent five different scaffolds: the isosteric benzofuropyrimidines **9a–c** and pyrimido-indoles **10a–c** scaffolds identified in the β_2R-based H_4R model, and bezo-imidazole **11**, triazoloquinoxaline **12**, and morpholinopyrimidine **13** identified in the H_1R-based H_4R model.

Discussion

Ligand- and protein-based virtual screening methods are complementary

One of the challenges in SBVFS is the limited experimental data on true inactive (fragment-like) compounds to properly validate and optimize virtual screening approaches. Our in-house fragment screening against H_4R provided invaluable data that enabled us to construct a balanced training set of true active and true inactive H_4R fragments.[14,17] The H_4R active fragments from our in-house screens[14,17] were appended by active fragment-like H_4R ligands from the ChEMBL database[77,101] to further increase the number of true H_4R active fragments. This dedicated training set of fragment-like compounds enabled us to retrospectively validate different ligand- and protein-based virtual fragment screening protocols (Fig. 1).

Both (2D and 3D) ligand-based and structure-based (IFP) virtual screening approaches gave good early enrichment in our retrospective virtual screening studies (Fig. 3, Table 1). SBVS using PLANTS scoring on the other hand resulted in significantly lower enrichments (Fig. 3, Table 1). Although 2D-LBVS gave high early enrichments, the global virtual screening accuracies (AUC values) of the ECFP-4 2D similarity searches were relatively low, indicating that this method is, as expected, rather dependent on the reference ligand. 3D-LBVS runs also gave high enrichments for the relatively larger reference ligands (Fig. 3, Table 1), and retrieved ligands that were not identified in 2D-LBVS simulations (Fig. 5). Enrichments obtained by 3D-similarity screens based on the relatively small histamine reference ligand (only 8 heavy atoms) are, however, significantly lower than 2D-similarity screens based on the same ligand (5-fold lower $EF_{1\%}$). This suggests that very small fragments are less distinguishable based on shape and electrostatic/pharmacophore similarity. Indeed,

Table 2 The biological activities and the prospective VS parameters of the H_4R confirmed hits identified employing β_2R-based H_4R homology model

Compounds	Biological activities ($pK_i \pm SEM$)[a]		Tc-IFP score[d] (#rank)		$PLANTS_{ChemPLP}$ score[e] (#rank)		ECFP4 similarity[f] (#rank)		Reference ROCS-EON[g] (#rank)		ECFP4 similarity[h]
	H_4R[b]	β_2R[c]	SBVS-1	SBVS-2	SBVS-1	SBVS-2	JNJ (2)	VUF (3)	JNJ (2)	VUF (3)	ChEMBL
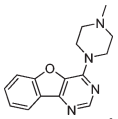 VUF13682 (**9a**)	6.84 ± 0.12	<5	—	0.909 (#14)	−90.759 (#4653)	−97.161 (#3550)	0.121 (#8124)	0.178 (#1790)	1.513 (#3945)	1.506 (#408)	0.254
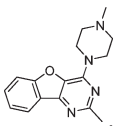 VUF13686 (**9b**)	6.83 ± 0.08	<5	0.750 (#4513)	0.909 (#10)	−76.260 (#25 334)	−99.754 (#2232)	0.119 (#8566)	0.178 (#1805)	1.519 (#3829)	1.513 (#352)	0.294
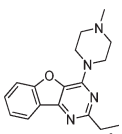 VUF13687 (**9c**)	6.57 ± 0.06	<5	0.750 (#4821)	0.909 (#6)	−68.907 (#36 530)	−101.757 (#1448)	0.113 (#10 241)	0.184 (#1462)	1.528 (#3651)	1.529 (#244)	0.268
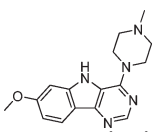 VUF13690 (**10a**)	5.20 ± 0.06	<5	1.000 (#1)	0.864 (#103)	−92.650 (#3285)	−95.021 (#4986)	0.139 (#5171)	0.192 (#1038)	1.565 (#2886)	1.527 (#257)	0.261
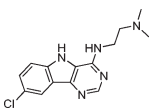 VUF13694 (**10b**)	5.23 ± 0.06	<5	0.842 (#418)	0.955 (#1)	−83.531 (#12 968)	−97.851 (#3129)	0.159 (#3191)	0.223 (#306)	1.653 (#1455)	1529 (#243)	0.319
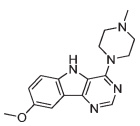 VUF13695 (**10c**)	5.23 ± 0.03	<5	0.810 (#777)	0.909 (#9)	−78.414 (#21 595)	−100.022 (#2097)	0.141 (#4888)	0.179 (#1721)	1.554 (#3102)	1.588 (#62)	0.286

[a] pK_i values are calculated from at least three independent measurements as the mean ± SEM. [b] Measured by displacement of [^{3}H]-histamine binding using membranes of HEK293T cells transiently expressing the human H_4R. [c] Measured by displacement of [^{3}H]-dihydroalprenolol binding using membranes of HEK293T cells transiently expressing the human β_2R. [d] IFP Tanimoto similarity with the pose of either JNJ7777120 (SBVS-1) or VUF10497 (SBVS-2) in the H_4R model. Tc-IFP ranking is given between brackets. [e] $PLANTS_{ChemPLP}$ docking score using H_4R model bound to JNJ7777120 (SBVS-1) or VUF10497 (SBVS-2). The ranking is given between brackets. [f] ECFP-4 2D Tanimoto similarity to JNJ7777120 (2), or VUF10497 (3). A similarity higher than 0.40 is considered as significant.[24] ECFP-4 ranking is given between brackets. [g] ROCS/EON shape/electrostatic-based 3D similarity to JNJ7777120 (2), or VUF10497 (3) based on Comboscore. A similarity higher than 1.30 is considered as significant. Comboscore ranking is given between brackets. [h] ECFP-4 circular fingerprint Tanimoto similarity to the closest known H_4R-active fragment used in the retrospective VS.[17,101] A similarity higher than 0.40 is considered as significant.[24]

histamine-based runs give relatively higher ROCS-EON scores (% of compounds within the database with a score ≥1.3 = 32%), than when using JNJ7777120 (26%) and VUF10497 (15%) as a reference. Another explanation could be that only disconnected groups are common between the reference and the target compound (maximum common edge (MCE) subgraph).[103] This is supported by the fact that 41% of the actives and 21% of the inactives share an imidazole ring with histamine. It should be noted that in a 3D-LBVS campaign, using JNJ7777120 (2) as the reference compound, new H_4R ligands were discovered[80] that are similar to the experimentally confirmed hits **9a–c** that were independently identified in our prospective SBVS study. These hit compounds from Cramp *et al.* were, however, not yet published when we performed our virtual screening and were therefore also not yet included in the ChEMBL database[77] version (downloaded on August 19, 2010) used in our study for the novelty assessment.

Structure-based virtual screening with a molecular interaction fingerprint (IFP) scoring method to rank PLANTS

Table 3 The biological activities and the prospective VS parameters of the H_4R confirmed hits identified employing H_1R-based H_4R homology model

Compounds	Biological activities (pK_i ± SEM)[a]		Tc-IFP score[d] (#rank)		$PLANTS_{ChemPLP}$ score[e] (#rank)		ECFP4 similarity[f] (#rank)		Reference ROCS-EON[g] (#rank)		ECFP4 similarity[h]
	H_4R[b]	H_1R[c]	SBVS-1	SBVS-2	SBVS-1	SBVS-2	JNJ (2)	VUF (3)	JNJ (2)	VUF (3)	ChEMBL
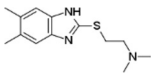 VUF13848 (**11**)	5.16 ± 0.03	<5[i]	0.800 (#413)	—	−83.836 (#2764)	−89.297 (#10 026)	0.125 (#71 765)	0.120 (#87 147)	1.635 (#6966)	1.380 (#5019)	0.200
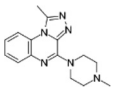 VUF13860 (**12**)	5.19 ± 0.07	>5[j]	0.727 (#3374)	—	−41.868 (#34 454)	−78.980 (#26 862)	0.215 (#12 441)	0.300 (#600)	1.624 (#8066)	1.563 (#142)	0.396
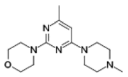 VUF13867 (**13**)	5.16 ± 0.04	>5[j]	—	0.739 (#626)	−74.071 (#12 599)	−93.292 (#1051)	0.213 (#13 059)	0.323 (#277)	1.643 (#6170)	1.472 (#1100)	0.264

[a] pK_i values are calculated from at least three independent measurements as the mean ± SEM. [b] Measured by displacement of [^{3}H]-histamine binding using membranes of HEK293T cells transiently expressing the human H_4R. [c] Measured by displacement of [^{3}H]-mepyramine binding using membranes of HEK293T cells transiently expressing the human H_1R. [d] IFP Tanimoto similarity with the pose of either JNJ7777120 (SBVS-1) or VUF10497 (SBVS-2) in the H_4R model. Tc-IFP ranking is given between brackets. [e] $PLANTS_{ChemPLP}$ docking score using H_4R model bound to JNJ7777120 (SBVS-1) or VUF10497 (SBVS-2). The ranking is given between brackets. [f] ECFP-4 2D Tanimoto similarity to JNJ7777120 (**2**), or VUF10497 (**3**). A similarity higher than 0.40 is considered as significant.[24] ECFP-4 ranking is given between brackets. [g] ROCS/EON shape/electrostatic-based 3D similarity to JNJ7777120 (**2**), or VUF10497 (**3**) based on Comboscore. A similarity higher than 1.30 is considered as significant.[102] Comboscore ranking is given between brackets. [h] ECFP-4 circular fingerprint Tanimoto similarity to the closest known H_4R active fragments used in the retrospective VS and the purchased hits based on β_2R-based prospective VS.[17,101] A similarity of higher than 0.40 is considered as significant.[24] [i] At 10 μM, the compounds showed [^{3}H]-mepyramine displacement of less than 50%. [j] At 10 μM, the compounds showed [^{3}H]-mepyramine displacement of more than 50%.

docking poses in JNJ7777120- and VUF10497-customized H_4R homology models (based on β_2R and H_1R crystal structure templates) gave comparably high enrichments as 2D and 3D ligand-based virtual screening methods (Fig. 3, Table 1). In fact, SBVS against the β_2R-based H_4R model refined with VUF10497 (**3**) gave the best early enrichment of all methods used in the retrospective evaluation. For both β_2R-based H_4R models higher retrospective virtual screening enrichments were obtained with VUF10497 (**3**) reference IFPs than with JNJ7777120 (**2**) or histamine (**1**) reference IFPs. A possible explanation for this result could be that the larger VUF10497 (**3**) ligand binds a larger part of the hydrophobic pocket between TM helices 3–6 (between $W316^{6.48}$, $Y319^{6.51}$, and $L175^{5.39}$) than JNJ777712 and histamine (Fig. 2). As a result the VUF10497 reference interaction fingerprint allows the retrieval of H_4R ligand docking poses that target the subpocket between $W316^{6.48}$ and $Y319^{6.51}$ and/or the subpocket between $Y319^{6.51}$ and $L175^{5.39}$, which may lead to a better enrichment in the retrospective SBVS studies.[36] It should furthermore be noted that VUF10497 (**3**) has the highest affinity compared to histamine (**1**) and JNJ7777120 (**2**).[7,8] Comparison of the overlap of ligands retrieved by the different methods furthermore shows that SBVS methods are capable of identifying of novel ligands that are chemically

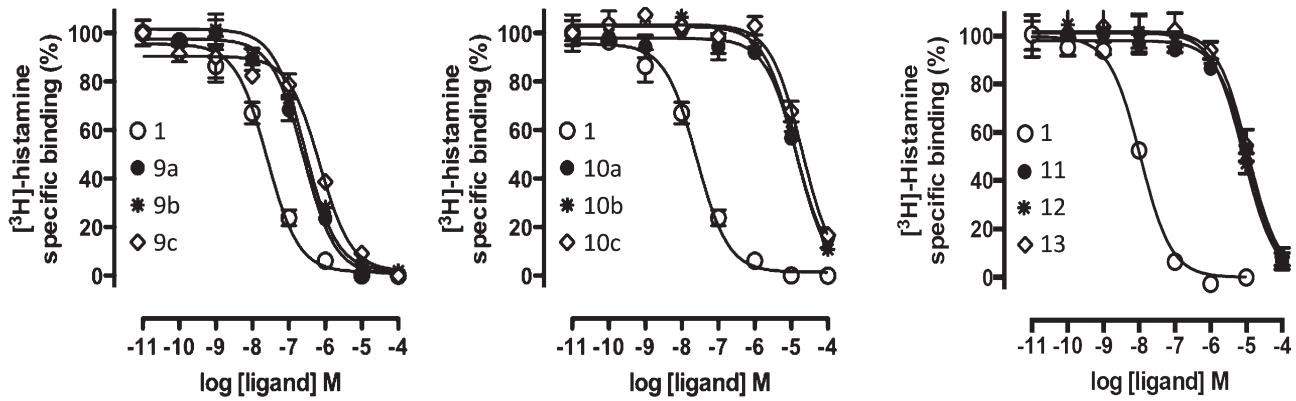

Fig. 6 [^{3}H]-histamine binding displacement by reference compound **1** and the nine virtual screening hits (**9a**–**c**, **10a**–**c**, **11**, **12**, **13**). Data shown are representative binding curves of at least three experiments performed in triplicate. Error bars indicate SEM values.

dissimilar from the ligands used to define the reference IFP that are not retrieved by 2D or 3D LBVS methods (Fig. 4). This indicates that ligand- and structure-based virtual screening methods are complementary as previously shown by Krüger and Evers.[29] Our results furthermore highlight the scaffold-hopping potential of SBVS in combination with IFP, as shown in previous studies.[24]

Structure-based virtual screening is an efficient way to identify novel fragment-like H_4R ligands

Based on the results of the retrospective VS studies (Table 1, Fig. 2–3), two β_2R-based H_4R models and their corresponding IFP references were used in prospective *in silico* screening runs to discover new active H_4R fragments from a subset of fragment-like and commercially-available molecules extracted from the ZINC database (Fig. 5). Six out of 23 purchased *in silico* hits were experimentally confirmed as active H_4R fragments with pK_i values of 5.2–6.8 (Table 2 and Fig. 7). By re-ranking the docking poses according to their IFP similarity the rank of the confirmed hits increased from #1448–#3550 for PLANTS to #1–#14 using IFP (Table 2). It should be noted that compounds **9a–c** (Table 2 and Fig. 7) is similar to the H_4R scaffold discovered by Cramp *et al.*[80] in an independent ligand-based virtual screening campaign. It should be emphasized however that the compounds discovered in this ligand-based screening were not yet included in the ChEMBLdb database[77] version used in our study,[101] and therefore were identified after completion of our own prospective structure-based virtual screening study.

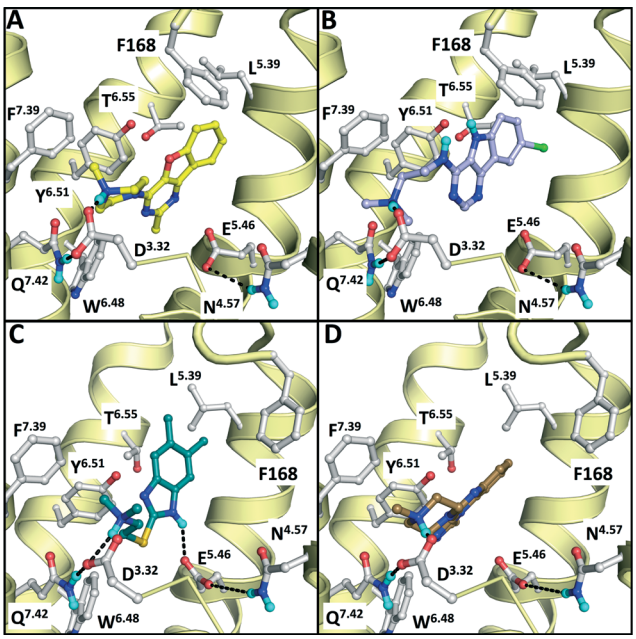

Fig. 7 Binding modes of the validated hits VUF13686 (**9b**, yellow, panel **A**) and VUF13694 (**10b**, purple, **B**) in the β_2R-based H_4R model, compared to the binding modes of VUF13848 (**11**, darkgreen, **C**), and VUF13860 (**12**, brown, **D**) in the H_1R-based H_4R model. Rendering is similar to Fig. 2.

We subsequently performed the prospective SBVS campaigns studies against the H_4R models that were built based on the H_1R crystal structure[45] (Fig. 3 and 5). The SBVS runs against the H_1R-based H_4R models identified three experimentally confirmed H_4R ligands (**11–13**) (Table 3, Fig. 6 and 7). These three additional ligands combine a basic amine moiety with scaffolds (bezo-imidazole **11**, triazoloquinoxaline **12**, morpholinopyrimidine **13**) that are different from the two isosteric H_4R ligand scaffolds (benzofuropyrimidines **9a–c** and pyrimido-indoles **10a–c**) discovered in the prospective SBVS campaigns against β_2R-based H_4R models (Tables 2–3, ESI† Fig. S5). Although the TM fold of the β_2R and H_1R crystal structure templates are similar,[44,45] the different EL2 loop conformations (in particular the orientation of F168) results in different H_4R models. As a result, the reference ligands (**2–3**) and the novel ligands identified in prospective virtual screening studies (**9–13**) have similar binding modes in β_2R based and H_4R models, including H-bond conserved H-bond interactions with $D94^{3.32}$ and $E182^{5.46}$, but adopt slightly different orientations in the EL2 region (Fig. 2 and 7). These subtle differences in both binding pocket structure and reference ligand binding mode result in relatively small differences in retrospective VS accuracies between H_4R homology models based on β_2R and H_1R crystal structure templates. Both modeling templates yield H_4R models with good early enrichments, but the retrospective virtual screening accuracy of the β_2R-based models is somewhat higher than the H_1R-based H_4R models (Table 1 and Fig. 2–3). Although the sequence identity between the H_4R and H_1R binding site is only slightly higher than between the H_4R and β_2R binding site,[23] H_1R is expected be a better template to model the EL2 region downstream from the conserved $C164^{EL2}$ that forms a disulphide bridge with $C77^{3.25}$ (including F168, ESI† Fig. S1). While H_1R-based H_4R models have previously been shown to better explain ligand SAR than β_2R-based H_4R homology models,[60] the current study indicates that the differences between H_1R and β_2R crystal structure templates does not significantly affect structure-based virtual screening accuracy of H_4R homology models. Moreover, prospective virtual screening studies against β_2R-based and H_1R-based H_4R models resulted both in the discovery of different new ligand chemotypes (Tables 2–3, Fig. 7–8). Our results are in line with recent comparative GPCR modeling studies which showed that comparable virtual screening results can be obtained with GPCR homology models and crystal structures.[25,27,39,40,104]

Notably, in contrast to the ligands found using β_2R-based H_4R models the confirmed hits discovered in the prospective SBVS campaigns against H_1R-based H_4R models were not the highest ranking compounds. Re-ranking the docking poses by their IFP similarity after the docking increased the rank of the confirmed hits from #1051–#26 862 using PLANTS to #413–#3374 using IFP (Table 3). This indicates that the post SBVS campaign steps presented in Fig. 5 (dissimilarity filter and visual inspection) has led to diverse sets of selected and purchased hits. The Venn Diagram of Fig. 8 shows the overlap between the hit lists obtained for each of the homology

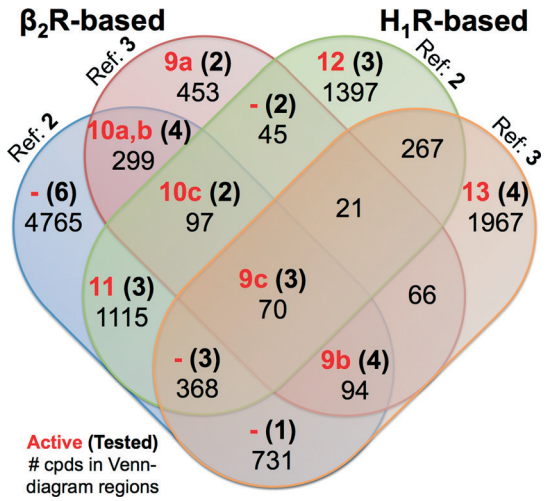

Fig. 8 Venn diagram showing the SBVS hit overlap for all prospectively applied homology models (see Fig. 5). The red bold numbers, the black bold numbers and the black regular numbers indicate the number of confirmed active hits (Tables 2 and 3), purchased hits (ESI† Figs. S4 and S5), and the number of hits after applying the IFP cutoffs, respectively.

models (after applying the retrospectively identified IFP score cutoffs, see Methods). The amount of unique ligands for each approach shows the complementarity of employing different modelling templates and different reference ligands to refine homology models. The purchased hits cover 12 out of 15 possible Venn-diagram regions, *i.e.* overlap combinations between homology-model hit lists (Fig. 8). Most of the confirmed active H_4R fragments were present in the hit lists of the VUF10497 models (7 out of 9). The remaining 2 confirmed H_4R fragments were identified in the SBVS using the H_1R-based model with JNJ7777120. None of the confirmed hits were unique for β_2R-based model with JNJ7777120, although one confirmed hit (VUF13848 (**11**)) was identified in both JNJ7777120 homology models.

Most of previous ligands designs for H_4R were highly inspired from the structure of JNJ7777120 (**2**)[4,59] since it was the first published non-imidazole antagonist for H_4R.[7] This might be the cause that the JNJ7777120 H_4R models resulted in more diverse selected active hits compared to the SBVS campaigns using VUF10497 (**3**) as the reference (Fig. 8). The $PLANTS_{ChemPLP}$ scores of the active H_4R fragments were higher (≤ -90)[24] in the SBVS with VUF10497 (**3**) as the reference compound (ESI† Fig. S6). The scoring distributions (Fig. S5) also show that with a lower PLANTS score the IFP score is increasing for only the VUF10497 models, which is in line with the finding that 7 out of the 9 confirmed hits were present in hit lists of these models. Hence, employing $PLANTS_{ChemPLP}$ score and Tc-IFP as a combined scoring function in SBVS campaigns could increase the SBVS quality (as it did for the aforementioned H_1R crystal structure-based VS),[24] but it depends on the structure models and the IFP references. Cut-offs optimization is therefore required to build SBVS protocols with optimized quality.

Similar to the SBVS on the H_1R crystal structure,[24] the combined approaches can lead in to a good hit rate (9 out of 36) of H_4R small fragments. Although the hit rate is lower than the SBVS on the H_1R crystal structure,[24] these results of the prospective virtual screening exercise validate our structure-based virtual fragment screening method.

Conclusions

We have investigated the possibilities of structure-based virtual fragment screening against optimized homology models of the histamine H_4R receptor. Structure- and ligand-based methods performed equally well in retrospective virtual screening studies, but structure-based virtual fragment screening using an interaction fingerprint scoring method enabled the identification of H_4R ligands that were not identified in ligand-based VS runs. Surprisingly, retrospective virtual screening validation studies against H_4R homology models based on the H_1R crystal structure did not give higher VS enrichments than H_4R models based on the crystal structure of the more distantly-related β_2R. Optimized SBVFS methods were successfully used to find two new series of fragment-like H_4R ligands. Nine out of the 37 tested compounds (representing five different scaffolds) had binding affinities between 0.14 and 6.9 μM at the H_4R. The results of our comparative study can be used to guide future structure-based virtual fragment screening campaigns.

Experimental section

Retrospective virtual screening

Residue numbering and nomenclature. The Ballesteros–Weinstein residue numbering scheme[105] was used throughout this manuscript. For explicitly numbered residues in specific receptors, the UniProt[106] residue number is given before the Ballesteros–Weinstein residue number in superscript (*e.g.*, $D94^{3.32}$ in H_4R).

Construction of retrospective validation database. Known H_4R active fragments were compiled from in-house libraries (defined as fragments that show more than 50% displacement of radioligand [^{3}H]histamine at 10 μM)[10,17] and ChEMBL database[77,101] (defined as fragment-like compounds with pK_i more than 7.0).[14] The inactive H_4R inactive fragments from in-house libraries (defined as fragments show less than 30% displacement of radioligand [^{3}H]histamine at 10 μM).[14,17] The tautomers and microspecies distributions at pH 7.4 of the ligands were generated by employing cxcalc tool of ChemAxon 5.2.5.1.[107] The species with abundance of more than 1% were selected. The 3D structures were generated using CORINA 3.46 subsequently.[108]

Construction and refinement H_4R homology models. Starting from a previously published 3D model of H_4R,[58,59,62] based on the β_2R crystal structure (PDB-code 2RH1),[44] new structural models of H_4R were constructed and refined by docking and molecular dynamics simulations with three representative H_4R ligands: Histamine (**1**), JNJ7777120 (**2**), and

VUF10497 (3). For each H_4R-ligand complex optimal structures were selected based on their ability to discriminate between known fragment-like H_4R ligands and true fragment-like H_4R inactives (see subsection *Construction of retrospective validation database*) in retrospective virtual screening studies. A second set of H_4R models was built based on the recently solved H_1R crystal structure (PDB-code 3RZE)[45] using Modeller (using the same protocol as the previously published β_2R-based H_4R model)[58,59,62] and subjected to the same optimization and validation protocols as the β_2R-based H_4R homology models. The reference compounds were docked using PLANTS version 1.1 into the H_4R binding pocket, which was defined using PLANTS bind tool.[93] The best pose of each reference was selected. The selected poses show interaction to $D94^{3.32}$ and $E182^{5.46}$ and have highest IFP similarity Tanimoto coefficient (Tc-IFP)[36,74] to the previously described 3D model of JNJ7777120 (2) in the H_4R.[58,59,62] The selected protein-ligand complex was then minimized using AMBER 10 to relax the structure.[109] Forcefield parameters for the ligands were derived using the Antechamber program and partial charges for the ligands were computed using the AM1-BCC procedure in Antechamber.[109] Upper-bound distance restraint of 3.5 Å to maintain the interaction of the ligand to $D^{3.32}$ was applied. The minimized model was subsequently embedded in a pre-equilibrated lipid bilayer consisting molecules of 1-palmitoyl-2-oleoyl-phosphatidylcholine (POPC) and solvated with TIP3P water molecules (box dimensions: 82.3 Å × 74.8 Å × 80.4 Å) as described by Urizar *et al.*[74,110] The complexes embedded in the hydrated lipid bilayer were minimized shortly using AMBER 10.[109] The hydrogen bond to $D^{3.32}$ constraint and a positional harmonic constraint of 50 kcal mol^{-1} Å on Cα carbon atoms were applied. The entire system was then subjected to a 1.1 ns constant pressure molecular dynamics (MD) simulation. All bonds involving hydrogen atoms were frozen with the SHAKE algorithm. During the first 100 ps, the Cα carbon atoms were constrained and the hydrogen bond of the ligand to $D^{3.32}$ was restrained as previously described and the temperature was linearly increased from 0 to 300 K. During the last 1000 ps, the temperature was kept constant at 300 K and the pressure at 1 bar, using a coupling constant of 0.2 ps and the Berendsen approach. Interactions were calculated according to the AMBER03 force field, using particle-mesh-Ewald (PME) summation to include the long range electrostratic forces. Van der Waals interactions were calculated using a cut-off of 8.0 Å. MD snapshots were clustered with the GROMACS g_cluster tool with respect to the Cα atoms of the defined binding residues and according to the Jarvis–Patrick method, using a cutoff of 3 Å for defining the nearest neighbours.[111] This yielded 3 to 8 clusters per simulation run. The binding pocket regions of MD snapshots were then fitted to the corresponding binding pocket regions of the initial 3D model. The MD-snapshots of the complexes were finally energy minimized as described before. The minimized ligand-protein complexes from the MD-snapshots were subjected to perform SBVS campaigns retrospectively using PLANTS docking software. The IFP for each docked pose was calculated subsequently. Pose with hydrogen bond to $D^{3.32}$ and highest Tc-IFP value for each ligand was selected. Early enrichment ($EF_{1\%}$) values derived from receiver operating characteristic (ROC) curves were used as virtual screening criteria to evaluate the applicability of the MD snapshots to discriminate between known fragment-like H_4R ligands and true fragment-like H_4R inactives (see subsection *Construction of retrospective validation database*) in retrospective virtual screening studies. Two best snapshots performing SBVS were used further in prospective virtual screening.

Automated docking. All virtual screenings were performed by docking program PLANTS (version 1.1).[112] PLANTS combines an ant colony optimization algorithm with an empirical scoring function for the prediction and scoring of binding poses in a protein structure.[93,112] For each compound, 15 poses were calculated and scored by the ChemPLP scoring function at speed setting 2. The binding pocket of H_4R was defined by the coordinates of the center of the reference ligand and a radius of 5 Å (which is the maximum distance from the center defined by a 5 Å radius around the reference ligand). All other options of PLANTS were left at their default setting. The same docking approach was used to dock experimentally confirmed hits in the H_1R crystal structure.[45]

IFP post-processing. The reference ligand binding modes in the corresponding H_4R-ligand complex models were used to generate reference interaction fingerprints (IFPs) as previously described.[36] Seven different interaction types (negatively charged, positively charged, H-bond acceptor, H-bond donor, aromatic face-to-edge, aromatic-face-to-face, and hydrophobic interactions) were used to define the IFP. The cavity used for the IFP analysis has been highlighted in ESI† Fig. S1.

Automated docking. Note that for each PLANTS docking pose, a unique subset of protein coordinates with rotated hydroxyl hydrogen atoms were used to define the IFP. Standard IFP scoring parameters, and a Tanimoto coefficient (Tc-IFP) measuring IFP similarity with the reference molecule pose of histamine (1), JNJ7777120 (2), and VUF10497 (3) in the H_4R models, was used to filter and rank the docking poses of 100 known fragment-like H_4R ligands, 959 fragment-like compounds that are inactive at H_4R, and the focused database of 23 112 fragment-like molecules (only poses forming an H-bond and ionic interaction with $D94^{3.32}$ are considered). For the H_4R confirmed hits presented in Tables 2 and 3, the docking protocols against H_1R crystal structure were performed.[24,45] The doxepin binding mode in the original H_1R X-ray structure[45] was used to generate reference IFP. The H_1R cavity used for the IFP analysis consisted the same set of 33 residues used in previously published SBVS studies.[24,73]

ROCS 3D similarity search. The conformer database was generated using standard settings OMEGA[113] and searched with ROCS[92] using standard settings as well. The conformations of histamine (1), JNJ7777120 (2), and VUF10497 (3) in the H_4R models were used as query molecules for

independent ROCS runs. Compounds were ranked by decreasing EON score[92] (combination of the shape and the electrostatic potential Tanimoto similarity in this optimized overlay). Score higher than 1.30 is considered as significant.[102]

ECFP-4 2D similarity search. Two-dimensional similarity searches were carried out using ECFP-4 (extended connectivity fingerprints)[98] descriptors available in Pipeline Pilot version 6.1.5 [114] and compared using the Tanimoto coefficient.

Retrospective virtual screening analysis. A hundred known fragment-like H_4R ligands[17,101] and 959 fragment-like compounds that are inactive at H_4R[17] were subjected to 2D-LBVS (ECFP-4)[98,114] and 3D-LBVS (ROCS-EON)[92] runs and docked into H_4R models and scored with PLANTS and IFP.[24,36,93,112] Virtual screening accuracies were first determined in terms of area under the curve of receiver–operator characteristic (ROC) plots, and its 95% confidence interval was computed with R statistical computing software version 2.11.1.[95,97] Enrichment in true positives (TP) is reported at a false positive rate (FP) of 1% ($EF_{1\%}$) as follows: $EF_{1\%} = TP/FP_{1\%}$. Early enrichment at 1% rate was computed for each virtual screen.[115]

Prospective virtual screening

Preparation of prospective virtual screening database. Similar procedures to create fragment database to perform prospective crystal structure based virtual screening to discover H_1R fragments were employed.[24] From 16 vendors we downloaded their commercial compound datasets in SMILES format from the ZINC website. With use of Openeye's filter (version 2.1.1),[39,116] only fragment-like compounds were selected (43 326 compounds). Plausible tautomers and protonation states at pH 7.4 were computed for these compounds with cxcalc tool of ChemAxon 5.2.5.1.[107] The species with abundance of more than 20% were selected. The 3D structures were generated using CORINA subsequently.[108,117] Second filter was applied to select only compounds with a formal charge of at least +1, this selection ensures that all selected compounds have the possibility for an ionic bond with key residue $D94^{3.32}$ in the pocket (42 620 compounds). Subsequently, third filter was applied to remaining compounds to select compounds which do not have plausible reactive groups.[100] This selection decreases the probability to have hits which can lead to be toxic compounds.[100]

SBVS on β_2R-based H_4R model. Prospective fragment virtual screenings were performed on compounds from ZINC database.[99] Fragment-like compounds,[10] which come from selected vendors in the database (ESI† Table S1) were selected. The tautomers and microspecies distributions at pH 7.4 of the ligands were generated as described in subsection *Preparation of prospective virtual screening database*. The species with abundance of more than 20% were selected. The 3D structures were then generated using CORINA as described in subsection *Preparation of prospective virtual screening database*.[108] The structures were objected to the SBVS campaigns using two selected MD snapshots (SBVS-1 and 2). The Tc-IFP values of enrichment factor of 1% ranked false positives ($EF_{1\%}$) of the selected SBVS protocols were used as the cut-offs: 0.733 and 0.810 for SBVS-1 and SBVS-2, respectively. To avoid similar scaffolds to the known H_4R fragments, the hits with ECFP-4 similarity values of less than 0.40 against all known H_4R active fragments used in the retrospective VS were selected and the remaining hits were subjected to visual inspection.[24] The compounds selected by virtual screening were purchased from available screening collections of 7 vendors (ESI† Tables S2 and S3). The purity of all compounds was verified by liquid chromatography-mass spectrometry (LC-MS). All experimentally validated hits had a purity of 96% or higher (see Table S4†).

SBVS on H_1R-based H_4R model. Subsequently, the similar protocol was used to virtually screen compounds against the models built based on H_1R crystal structures.[45] The differences are: (i) The Tc-IFP values of enrichment factor of 1% ranked false positives ($EF_{1\%}$) of the selected SBVS protocols were used as the cut-offs: 0.727 and 0.714 for SBVS-1 and SBVS-2, respectively; and (ii) The selected and purchased H_4R hits resulted from the SBVS on β_2R-based H_4R models were added in the dissimilarity filtering.

Pharmacological assays

HEK293T cells were cultured in Dulbecco's modified Eagle medium (DMEM) supplemented with 10% fetal bovine serum, 50 IU ml^{-1} penicillin and 50 μg ml^{-1} streptomycin at 37 °C and 5% CO_2. Approximately 4×10^6 cells in 10 cm dishes were transiently transfected with 5 μg receptor DNA using 25 kDa linear polyethylenimine (PEI; Polysciences, Warrington, USA) as transfection reagent (1 : 4 DNA/PEI ratio). The cells were harvested 2 days after transfection and homogenized in 50 mM Tris-HCl binding buffer (pH 7.4). Cell homogenates were co-incubated with indicated concentrations of compounds and ~3 nM [^{3}H]-mepyramine (human H_1R), ~10 nM [^{3}H]-histamine (human H_4R), or ~2 nM [^{3}H]-dihydroalprenolol (human β_2R) in a total volume of 100 μl per well. All radioligands were purchased from PerkinElmer Life Sciences. The reaction mixtures were incubated for 1–1.5 h at 25 °C on a microtiter shaker (750 rpm). Incubations were terminated by rapid filtration through Unifilter glass fiber C plates (PerkinElmer Life Sciences) that were presoaked in 0.3% polyethylenimine and subsequently washed three times with ice-cold binding buffer (pH 7.4 at 4 °C). Retained radioactivity was measured by liquid scintillation using a MicroBeta Trilux (PerkinElmer Life Sciences). Nonlinear curve fitting was performed using GraphPad Prism version 6.00 for Windows/Mac OSX, GraphPad Software, La Jolla California USA, www.graphpad.com. The K_i values were calculated using the Cheng–Prusoff equation:[118] $K_i = IC_{50}/(1 + [\text{radioligand}]/K_d)$.

Acknowledgements

We thank Mitchell K. L. Han for assistance with radioligand displacement and Antoni R. Blaazer for performing the

quality control of the compounds. This research was financially supported by The Netherlands Organization for Scientific Research (NWO VENI Grant 700.59.408 to C. d. G. and NWO TOP PUNT Grant to R. L.), Indonesian Directorate General of Higher Education (Fundamental Research Block Grant 1320/K5/KM/2014 to E. P. I.) and Institute for Research and Community Services, Sanata Dharma University (Research Grant 083/Panel/LPPM-USD/SP/X/2013 to E. P. I). A. J. K., H. F. V., S. N., I. J. P. d. E., R. L., and C. d. G. participate in the European Cooperation in Science and Technology Action CM1207 [GPCR-Ligand Interactions, Structures, and Transmembrane Signalling: A European Research Network (GLISTEN)].

Notes and references

1 M. C. Lagerström and H. B. Schiöth, *Nat. Rev. Drug Discovery*, 2008, **7**, 339–357.
2 R. Leurs, H. F. Vischer, M. Wijtmans and I. J. P. de Esch, *Trends Pharmacol. Sci.*, 2011, **32**, 250–257.
3 H. D. Lim, R. A. Smits, R. Leurs and I. J. P. de Esch, *Curr. Top. Med. Chem.*, 2006, **6**, 1365–1373.
4 E. P. Istyastono, C. de Graaf, I. J. P. de Esch and R. Leurs, *Curr. Top. Med. Chem.*, 2011, **11**, 661–679.
5 R. A. Smits, R. Leurs and I. J. P. de Esch, *Drug Discovery Today*, 2009, **14**, 745–753.
6 H. Engelhardt, R. A. Smits, R. Leurs, E. Haaksma and I. J. P. de Esch, *Curr. Opin. Drug Discovery Dev.*, 2009, **12**, 628–643.
7 J. A. Jablonowski, C. A. Grice, W. Chai, C. A. Dvorak, J. D. Venable, A. K. Kwok, K. S. Ly, J. Wei, S. M. Baker, P. J. Desai, W. Jiang, S. J. Wilson, R. L. Thurmond, L. Karlsson, J. P. Edwards, T. W. Lovenberg and N. I. Carruthers, *J. Med. Chem.*, 2003, **46**, 3957–3960.
8 R. A. Smits, I. J. P. de Esch, O. P. Zuiderveld, J. Broeker, K. Sansuk, E. Guaita, G. Coruzzi, M. Adami, E. Haaksma and R. Leurs, *J. Med. Chem.*, 2008, **51**, 7855–7865.
9 D. A. Erlanson, R. S. McDowell and T. O'Brien, *J. Med. Chem.*, 2004, **47**, 3463–3482.
10 G. E. de Kloe, D. Bailey, R. Leurs and I. J. P. de Esch, *Drug Discovery Today*, 2009, **14**, 630–646.
11 C. W. Murray, M. L. Verdonk and D. C. Rees, *Trends Pharmacol. Sci.*, 2012, **33**, 224–232.
12 M. Congreve, R. Carr, C. Murray and H. Jhoti, *Drug Discovery Today*, 2003, **8**, 876–877.
13 S. M. Boyd and G. E. de Kloe, *Drug Discovery Today: Technol.*, 2010, **7**, e173–e180.
14 C. de Graaf, H. F. Vischer, G. E. de Kloe, A. J. Kooistra, S. Nijmeijer, M. Kuijer, M. H. Verheij, P. J. England, J. E. van Muijlwijk-Koezen, R. Leurs and I. J. de Esch, *Drug Discovery Today*, 2013, **18**, 323–330.
15 A. R. Leach and M. M. Hann, *Curr. Opin. Chem. Biol.*, 2011, **15**, 489–496.
16 M. Congreve, R. L. Rich, D. G. Myszka, F. Figaroa, G. Siegal and F. H. Marshall, *Methods Enzymol.*, 2011, **493**, 115–136.
17 M. H. P. Verheij, C. de Graaf, G. E. de Kloe, S. Nijmeijer, H. F. Vischer, R. A. Smits, O. P. Zuiderveld, S. Hulscher, L. Silvestri, A. J. Thompson, J. E. van Muijlwijk-Koezen, S. C. R. Lummis, R. Leurs and I. J. P. de Esch, *Bioorg. Med. Chem. Lett.*, 2011, **21**, 5460–5464.
18 A. Visegrady and G. M. Keseru, *Expert Opin. Drug Discovery*, 2013, **8**, 811–820.
19 D. Chen, J. C. Errey, L. H. Heitman, F.H. Marshall, A. P. Ijzerman and G. Siegal, *ACS Chem. Biol.*, 2012, **7**, 2064–2073.
20 D. Chen, A. Ranganathan, I. J. AP, G. Siegal and J. Carlsson, *J. Chem. Inf. Model.*, 2013, **53**, 2701–2714.
21 J. A. Christopher, J. Brown, A. S. Dore, J. C. Errey, M. Koglin, F. H. Marshall, D. G. Myszka, R. L. Rich, C. G. Tate, B. Tehan, T. Warne and M. Congreve, *J. Med. Chem.*, 2013, **56**, 3446–3455.
22 S. P. Andrews, G. A. Brown and J. A. Christopher, *ChemMedChem*, 2014, **9**, 256–275.
23 A. J. Kooistra, S. Kuhne, I. J. de Esch, R. Leurs and C. de Graaf, *Br. J. Pharmacol.*, 2013, **170**, 101–126.
24 C. de Graaf, A. J. Kooistra, H. F. Vischer, V. Katritch, M. Kuijer, M. Shiroishi, S. Iwata, T. Shimamura, R. C. Stevens, I. J. de Esch and R. Leurs, *J. Med. Chem.*, 2011, **54**, 8195–8206.
25 F. Sirci, E. P. Istyastono, H. F. Vischer, A. J. Kooistra, S. Nijmeijer, M. Kuijer, M. Wijtmans, R. Mannhold, R. Leurs, I. J. P. de Esch and C. de Graaf, *J. Chem. Inf. Model.*, 2012, **52**, 3308–3324.
26 M. Vass, É. Schmidt, F. Horti and G. M. Keserű, *Eur. J. Med. Chem.*, 2014, **77**, 38–46.
27 A. J. Kooistra, R. Leurs, I. J. P. de Esch and C. de Graaf, *Adv. Exp. Med. Biol.*, 2014, **796**, 129–157.
28 J. Venhorst, S. Nunez, J. W. Terpstra and C. G. Kruse, *J. Med. Chem.*, 2008, **51**, 3222–3229.
29 D. M. Krüger and A. Evers, *ChemMedChem*, 2010, **5**, 148–158.
30 A. J. Kooistra, L. Roumen, R. Leurs, I. J. P. de Esch and C. de Graaf, *Methods Enzymol.*, 2013, **522**, 279–336.
31 N. Moitessier, P. Englebienne, D. Lee, J. Lawandi and C. R. Corbeil, *Br. J. Pharmacol.*, 2008, **153**(Suppl 1), S7–26.
32 M. Michino, E. Abola, GPCR Dock 2008 participants, C. L. Brooks 3rd, J. S. Dixon, J. Moult and R. C. Stevens, *Nat. Rev. Drug Discovery*, 2009, **8**, 455–463.
33 I. Kufareva, M. Rueda, V. Katritch, R. C. Stevens, R. Abagyan and GPCR Dock 2010 participants, *Structure*, 2011, **19**, 1108–1126.
34 A. Tarcsay, G. Paragi, M. Vass, B. Jójárt, F. Bogár and G. M. Keserű, *J. Chem. Inf. Model.*, 2013, **53**, 2990–2999.
35 I. Kufareva, V. Katritch, GPCR Dock 2013 participants, R. C. Stevens and R. Abagyan, *Structure*, 2014, **22**, 1120–1139.
36 G. Marcou and D. Rognan, *J. Chem. Inf. Model.*, 2007, **47**, 195–207.
37 K. Loving, I. Alberts and W. Sherman, *Curr. Top. Med. Chem.*, 2010, **10**, 14–32.
38 M. L. Verdonk, I. Giangreco, R. J. Hall, O. Korb, P. N. Mortenson and C. W. Murray, *J. Med. Chem.*, 2011, **54**, 5422–5431.
39 J. Carlsson, R. G. Coleman, V. Setola, J. J. Irwin, H. Fan, A. Schlessinger, A. Sali, B. L. Roth and B. K. Shoichet, *Nat. Chem. Biol.*, 2011, **7**, 769–778.

40 S. Vilar, G. Ferino, S. S. Phatak, B. Berk, C. N. Cavasotto and S. Costanzi, *J. Mol. Graphics Modell.*, 2011, **29**, 614–623.
41 V. Katritch, V. Cherezov and R. C. Stevens, *Annu. Rev. Pharmacol. Toxicol.*, 2013, **53**, 531–556.
42 A. J. Venkatakrishnan, X. Deupi, G. Lebon, C. G. Tate, G. F. Schertler and M. M. Babu, *Nature*, 2013, **494**, 185–194.
43 A. J. Kooistra, C. de Graaf and H. Timmerman, *Neurochem. Res.*, 2014, **39**, 1850–1861.
44 V. Cherezov, D. M. Rosenbaum, M. A. Hanson, S. G. Rasmussen, F. S. Thian, T. S. Kobilka, H. J. Choi, P. Kuhn, W. I. Weis, B. K. Kobilka and R. C. Stevens, *Science*, 2007, **318**, 1258–1265.
45 T. Shimamura, M. Shiroishi, S. Weyand, H. Tsujimoto, G. Winter, V. Katritch, R. Abagyan, V. Cherezov, W. Liu, G. W. Han, T. Kobayashi, R. C. Stevens and S. Iwata, *Nature*, 2011, **475**, 65–70.
46 P. Kolb, D. M. Rosenbaum, J. J. Irwin, J. J. Fung, B. K. Kobilka and B. K. Shoichet, *Proc. Natl. Acad. Sci. U. S. A.*, 2009, **106**, 6843–6848.
47 V. Katritch, V. P. Jaakola, J. R. Lane, J. Lin, A. P. Ijzerman, M. Yeager, I. Kufareva, R. C. Stevens and R. Abagyan, *J. Med. Chem.*, 2010, **53**, 1799–1809.
48 J. Carlsson, L. Yoo, Z. Gao, J. J. Irwin, B. K. Shoichet and K. A. Jacobson, *J. Med. Chem.*, 2010, **53**, 3748–3755.
49 D. Rodriguez, J. Brea, M. I. Loza and J. Carlsson, *Structure*, 2014, **22**, 1140–1151.
50 J. Varady, X. Wu, X. Fang, J. Min, Z. Hu, B. Levant and S. Wang, *J. Med. Chem.*, 2003, **46**, 4377–4392.
51 A. Evers and T. Klabunde, *J. Med. Chem.*, 2005, **48**, 1088–1097.
52 M. Congreve, J. M. Dias and F. H. Marshall, *Prog. Med. Chem.*, 2014, **53**, 1–63.
53 K. A. Jacobson and S. Costanzi, *Mol. Pharmacol.*, 2012, **82**, 361–371.
54 N. Shin, E. Coates, N. J. Murgolo, K. L. Morse, M. Bayne, C. D. Strader and F. J. Monsma, *Mol. Pharmacol.*, 2002, **62**, 38–47.
55 A. Jongejan, H. D. Lim, R. A. Smits, I. J. de Esch, E. Haaksma and R. Leurs, *J. Chem. Inf. Model.*, 2008, **48**, 1455–1463.
56 R. Kiss, B. Kiss, A. Konczol, F. Szalai, I. Jelinek, V. Laszlo, B. Noszal, A. Falus and G. M. Keseru, *J. Med. Chem.*, 2008, **51**, 3145–3153.
57 Y. Tanrikulu, E. Proschak, T. Werner, T. Geppert, N. Todoroff, A. Klenner, T. Kottke, K. Sander, E. Schneider, R. Seifert, H. Stark, T. Clark and G. Schneider, *ChemMedChem*, 2009, **4**, 820–827.
58 H. D. Lim, C. de Graaf, W. Jiang, P. Sadek, P. M. McGovern, E. P. Istyastono, R. A. Bakker, I. J. de Esch, R. L. Thurmond and R. Leurs, *Mol. Pharmacol.*, 2010, **77**, 734–743.
59 E. P. Istyastono, S. Nijmeijer, H. D. Lim, A. van de Stolpe, L. Roumen, A. J. Kooistra, H. F. Vischer, I. J. de Esch, R. Leurs and C. de Graaf, *J. Med. Chem.*, 2011, **54**, 8136–8147.
60 S. Schultes, S. Nijmeijer, H. Engelhardt, A. J. Kooistra, H. F. Vischer, I. J. P. de Esch, E. E. J. Haaksma, R. Leurs and C. de Graaf, *Med. Chem. Commun.*, 2013, **4**, 193.
61 S. Schultes, H. Engelhardt, L. Roumen, O. P. Zuiderveld, E. E. Haaksma, I. J. de Esch, R. Leurs and C. de Graaf, *ChemMedChem*, 2013, **8**, 49–53.
62 M. Wijtmans, C. de Graaf, G. de Kloe, E. P. Istyastono, J. Smit, H. Lim, R. Boonnak, S. Nijmeijer, R. A. Smits, A. Jongejan, O. Zuiderveld, I. J. P. de Esch and R. Leurs, *J. Med. Chem.*, 2011, **54**, 1693–1703.
63 R. A. Smits, M. Adami, E. P. Istyastono, O. P. Zuiderveld, C. M. van Dam, F. J. de Kanter, A. Jongejan, G. Coruzzi, R. Leurs and I. J. de Esch, *J. Med. Chem.*, 2010, **53**, 2390–2400.
64 T. Warne, M. J. Serrano-Vega, J. G. Baker, R. Moukhametzianov, P. C. Edwards, R. Henderson, A. G. Leslie, C. G. Tate and G. F. Schertler, *Nature*, 2008, **454**, 486–491.
65 E. Y. Chien, W. Liu, Q. Zhao, V. Katritch, G. W. Han, M. A. Hanson, L. Shi, A. H. Newman, J. A. Javitch, V. Cherezov and R. C. Stevens, *Science*, 2010, **330**, 1091–1095.
66 K. Haga, A. C. Kruse, H. Asada, T. Yurugi-Kobayashi, M. Shiroishi, C. Zhang, W. I. Weis, T. Okada, B. K. Kobilka, T. Haga and T. Kobayashi, *Nature*, 2012, **482**, 547–551.
67 A. C. Kruse, J. Hu, A. C. Pan, D. H. Arlow, D. M. Rosenbaum, E. Rosemond, H. F. Green, T. Liu, P. S. Chae, R. O. Dror, D. E. Shaw, W. I. Weis, J. Wess and B. K. Kobilka, *Nature*, 2012, **482**, 552–556.
68 C. Wang, Y. Jiang, J. Ma, H. Wu, D. Wacker, V. Katritch, G. W. Han, W. Liu, X. P. Huang, E. Vardy, J. D. McCorvy, X. Gao, X. E. Zhou, K. Melcher, C. Zhang, F. Bai, H. Yang, L. Yang, H. Jiang, B. L. Roth, V. Cherezov, R. C. Stevens and H. E. Xu, *Science*, 2013, **340**, 610–614.
69 S. Topiol and M. Sabio, *Bioorg. Med. Chem. Lett.*, 2008, **18**, 1598–1602.
70 D. R. Weiss, S. Ahn, M. F. Sassano, A. Kleist, X. Zhu, R. Strachan, B. L. Roth, R. J. Lefkowitz and B. K. Shoichet, *ACS Chem. Biol.*, 2013, **8**, 1018–1026.
71 A. J. Kooistra, I. J. de Esch, R. Leurs and C. de Graaf, *PhD Thesis*, VU University Amsterdam, 2015.
72 M. M. Mysinger, D. R. Weiss, J. J. Ziarek, S. Gravel, A. K. Doak, J. Karpiak, N. Heveker, B. K. Shoichet and B. F. Volkman, *Proc. Natl. Acad. Sci. U. S. A.*, 2012, **109**, 5517–5522.
73 D. Rognan, *Top. Curr. Chem.*, 2012, **317**, 201–222.
74 C. de Graaf, N. Foata, O. Engkvist and D. Rognan, *Proteins*, 2008, **71**, 599–620.
75 G. Hessler and K.-H. Baringhaus, *Drug Discovery Today: Technol.*, 2010, **7**, e263–e269.
76 S. Schultes, A. J. Kooistra, H. F. Vischer, S. Nijmeijer, E. Haaksma, R. Leurs, I. J. P. de Esch and C. de Graaf, *J. Chem. Inf. Model.*, 2015, DOI: 10.1021/ci500694c.
77 A. Gaulton, L. J. Bellis, A. P. Bento, J. Chambers, M. Davies, A. Hersey, Y. Light, S. McGlinchey, D. Michalovich, B. Al-Lazikani and J. P. Overington, *Nucleic Acids Res.*, 2012, **40**, D1100–1107.
78 S. Nijmeijer, H. F. Vischer, E. M. Rosethorne, S. J. Charlton and R. Leurs, *Mol. Pharmacol.*, 2012, **82**, 1174–1182.
79 S. Nijmeijer, H. F. Vischer, F. Sirci, S. Schultes, H. Engelhardt, C. de Graaf, E. M. Rosethorne, S. J. Charlton and R. Leurs, *Br. J. Pharmacol.*, 2013, **170**, 78–88.

80 S. Cramp, H. J. Dyke, C. Higgs, D. E. Clark, M. Gill, P. Savy, N. Jennings, S. Price, P. M. Lockey, D. Norman, S. Porres, F. Wilson, A. Jones, N. Ramsden, R. Mangano, D. Leggate, M. Andersson and R. Hale, *Bioorg. Med. Chem. Lett.*, 2010, **20**, 2516–2519.
81 H. D. Lim, R. M. V. Rijn, P. Ling, R. A. Bakker, R. L. Thurmond and R. Leurs, *J. Pharmacol. Exp. Ther.*, 2005, **314**, 1310–1321.
82 S. Nijmeijer, H. Engelhardt, S. Schultes, A. C. van de Stolpe, V. Lusink, C. de Graaf, M. Wijtmans, E. E. Haaksma, I. J. de Esch, K. Stachurski, H. F. Vischer and R. Leurs, *Br. J. Pharmacol.*, 2013, **170**, 89–100.
83 J. A. Salon, D. T. Lodowski and K. Palczewski, *Pharmacol. Rev.*, 2011, **63**, 901–937.
84 D. Wacker, G. Fenalti, M. A. Brown, V. Katritch, R. Abagyan, V. Cherezov and R. C. Stevens, *J. Am. Chem. Soc.*, 2010, **132**, 11443–11445.
85 H. D. Lim, A. Jongejan, R. A. Bakker, E. Haaksma, I. J. de Esch and R. Leurs, *J. Pharmacol. Exp. Ther.*, 2008, **327**, 88–96.
86 M. Govoni, H. D. Lim, D. El-Atmioui, W. M. P. B. Menge, H. Timmerman, R. A. Bakker, R. Leurs and I. J. P. De Esch, *J. Med. Chem.*, 2006, **49**, 2549–2557.
87 B. M. Savall, J. P. Edwards, J. D. Venable, D. J. Buzard, R. Thurmond, M. Hack and P. McGovern, *Bioorg. Med. Chem. Lett.*, 2010, **20**, 3367–3371.
88 E. M. Rosethorne and S. J. Charlton, *Mol. Pharmacol.*, 2011, **79**, 749–757.
89 R. Seifert, E. H. Schneider, S. Dove, I. Brunskole, D. Neumann, A. Strasser and A. Buschauer, *Mol. Pharmacol.*, 2011, **79**, 631–638.
90 D. Wifling, K. Löffel, U. Nordemann, A. Strasser, G. Bernhardt, S. Dove, R. Seifert and A. Buschauer, *Br. J. Pharmacol.*, 2015, **172**, 785–798.
91 D. Rogers and M. Hahn, *J. Chem. Inf. Model.*, 2010, **50**, 742–754.
92 OpenEye Scientific Software Inc., 2009, ROCS version 2.3.1, Santa Fe. http://www.eyesopen.com.
93 O. Korb, T. Stützle and T. E. Exner, *J. Chem. Inf. Model.*, 2009, **49**, 84–96.
94 C. de Graaf and D. Rognan, *Curr. Pharm. Des.*, 2009, **15**, 4026–4048.
95 R Development Core Team, 2008, R: A Language and Environment for Statistical Computing, Vienna. http://www.r-project.org.
96 M. H. Zweig and G. Campbell, *Clin. Chem.*, 1993, **39**, 561–577.
97 X. Robin, N. Turck, A. Hainard, N. Tiberti, F. Lisacek, J.-C. Sanchez and M. Müller, *BMC Bioinf.*, 2011, **12**, 77.
98 A. Steffen, T. Kogej, C. Tyrchan and O. Engkvist, *J. Chem. Inf. Model.*, 2009, **49**, 338–347.
99 J. J. Irwin and B. K. Shoichet, *J. Chem. Inf. Model.*, 2005, **45**, 177–182.
100 T. I. Oprea, *J. Comput. Mol. Des.*, 2000, **14**, 251–264.
101 European Bioinformatics Institute, ChEMBLdb, 2010, Cambridgeshire. https://www.ebi.ac.uk/chembldb Accessed 19 August 2010.
102 A. B. Yongye, J. R. Appel, M. A. Giulianotti, C. T. Dooley, J. L. Medina-Franco, A. Nefzi, R. A. Houghten and K. Martínez-Mayorga, *Bioorg. Med. Chem.*, 2009, **17**, 5583–5597.
103 J. W. Raymond, E. J. Gardiner and P. Willett, *J. Chem. Inf. Comput. Sci.*, 2002, **42**, 305–316.
104 J. C. Mobarec, R. Sanchez and M. Filizola, *J. Med. Chem.*, 2009, **52**, 5207–5216.
105 J. A. Ballesteros and H. Weinstein, *Methods Neurosci.*, 1995, **25**, 366–428.
106 C. H. Wu, R. Apweiler, A. Bairoch, D. A. Natale, W. C. Barker, B. Boeckmann, S. Ferro, E. Gasteiger, H. Huang, R. Lopez, M. Magrane, M. J. Martin, R. Mazumder, C. O'Donovan, N. Redaschi and B. Suzek, *Nucleic Acids Res.*, 2006, **34**, D187–D191.
107 ChemAxon, 2009, MarvinBeans 5.2.5.1, Budapest.
108 Molecular Networks GmbH., 2008, Corina version 3.46, Erlangen, http://www.molecular-networks.com/products/corina.
109 D. A. Case, T. A. Darden, T. E. Cheatham III, C. L. Simmerling, J. Wang, R. E. Duke, R. Luo, M. Crowley, R. C. Walker, W. Zhang, K. M. Merz, B. Wang, S. Hayik, A. Roitberg, G. Seabra, I. Kolossváry, K. F. Wong, F. Paesani, J. Vanicek, X. Wu, S. R. Brozell, T. Steinbrecher, H. Gohlke, L. Yang, C. Tan, J. Mongan, V. Hornak, G. Cui, D. H. Mathews, M. G. Seetin, C. Sagui, V. Babin and P. A. Kollman, *Amber 10*, University of California, San Francisco, 2008.
110 E. Urizar, S. Claeysen, X. Deupí, C. Govaerts, S. Costagliola, G. Vassart and L. Pardo, *J. Biol. Chem.*, 2005, **280**, 17135–17141.
111 D. Van Der Spoel, E. Lindahl, B. Hess, G. Groenhof, A. E. Mark and H. J. C. Berendsen, *J. Comput. Chem.*, 2005, **26**, 1701–1718.
112 O. Korb, T. Stützle and T. E. Exner, *Proc. IEEE Swarm Intell. Symp.*, 2007, **1**, 115–134.
113 OpenEye Scientific Software Inc., 2008, OMEGA version 2.3.2, Santa Fe. http://www.eyesopen.com.
114 Accelrys, 2007, Pipeline Pilot version 6.1.5,San Diego. http://accelrys.com/products/pipeline-pilot.
115 A. N. Jain and A. Nicholls, *J. Comput.-Aided Mol. Des.*, 2008, **22**, 133–139.
116 OpenEye Scientific Software Inc., 2009, FILTER version 2.1.1, Santa Fe. http://www.eyesopen.com.
117 J. Sadowski, J. Gasteiger and G. Klebe, *J. Chem. Inf. Model.*, 1994, **34**, 1000–1008.
118 Y. Cheng and W. H. Prusoff, *Biochem. Pharmacol.*, 1973, **22**, 3099–3108.